Solar Biomass Gasification Combined With Iron Oxide Reduction for Syngas Production and Green Iron Metallurgy

Quentin Bellouard, Sylvain Rodat, Maguelone Grateau, Stéphane Abanades

frontiers in Energy Research

ORIGINAL RESEARCH
published: 28 April 2020
doi: 10.3389/fenrg.2020.00066

Solar Biomass Gasification Combined With Iron Oxide Reduction for Syngas Production and Green Iron Metallurgy

Quentin Bellouard[1,2,3], *Sylvain Rodat*[1]*, *Maguelone Grateau*[2,4] *and Stéphane Abanades*[1]

[1] Processes, Materials and Solar Energy Laboratory, PROMES-CNRS, Font-Romeu-Odeillo-Via, France, [2] Univ. Grenoble Alpes, Grenoble, France, [3] CEA-LITEN High Temperature Solar systems Laboratory (LSHT), Grenoble, France, [4] CEA-LITEN Dry Process Thermoconversion of Carboneous Resources Laboratory (L2CS), Grenoble, France

The solar gasification of biomass with iron oxide for combined syngas and iron production was investigated. Both solar energy and biomass are promising renewable energies. The process of gasification converts solid carbonaceous feedstocks into either fuels or chemicals. However, conventional processes require partial combustion of the feedstock for energy supply and inherently suffer from high oxygen production costs and low syngas calorific value due to dilution with combustion products. Chemical looping gasification using solid oxides is an alternative option to tackle these issues. By supplying concentrated solar energy as the high-temperature heat source, it is possible to produce even more syngas from the process while enabling solar energy storage into dispatchable fuels. This work proposes to explore solar biomass gasification over iron oxide at high heating rates, representative of the conditions obtained in solar reactors. Thermodynamic equilibriums of gasification reactions between 100 and 1,500°C were calculated and experimental results obtained at 1,100°C with a specially designed induction furnace were reported for biomass gasification with iron oxide, water, or carbon dioxide as oxidizing agents. Solid products analysis showed that iron oxide can be reduced to metallic iron depending on the proportion of the oxygen carrier. These results indicate that iron oxide is an effective material for solar biomass gasification producing both syngas and iron via a novel green metallurgical process.

Keywords: solar energy, chemical looping gasification, green metallurgy, iron oxide, biomass

OPEN ACCESS

Edited by:
Alfonso Chinnici,
University of Adelaide, Australia

Reviewed by:
Mohsen Sarafraz,
University of Adelaide, Australia
Reynaldo Palacios-Bereche,
Federal University of ABC, Brazil

***Correspondence:**
Sylvain Rodat
sylvain.rodat@promes.cnrs.fr

Specialty section:
This article was submitted to Process and Energy Systems Engineering, a section of the journal Frontiers in Energy Research

Received: *13 February 2020*
Accepted: *03 April 2020*
Published: *28 April 2020*

Citation:
Bellouard Q, Rodat S, Grateau M and Abanades S (2020) Solar Biomass Gasification Combined With Iron Oxide Reduction for Syngas Production and Green Iron Metallurgy. Front. Energy Res. 8:66. doi: 10.3389/fenrg.2020.00066

INTRODUCTION

Climate change due to greenhouse gases emissions is one of the main current challenges of our society. The transition from a fossil-based economy to renewable energies is ongoing. Research is very active in this field in order to develop a new energy model. Biomass gasification has been identified as a promising pathway toward the production of renewable fuels with limited greenhouse gas emissions (Kumar et al., 2009; Codina Gironès et al., 2018). The conventional autothermal process needs to burn about 1/3 of the raw biomass feedstock to provide the enthalpy of the reaction. It requires either upstream air separation units (oxy-combustion) or downstream gas separation if air is used as oxidizer or gasification agent, as the products are diluted into nitrogen. In order to supply the required heat, concentrated solar energy has been considered to

eliminate combustion and products contamination, while the high achievable temperatures and heating rates lead to high quality syngas with no CO_2 emission and solar energy is stored into chemical form (Nzihou et al., 2012; Loutzenhiser and Muroyama, 2017). Three main solar reactor concepts have been tested previously (Piatkowski et al., 2011): indirectly irradiated packed bed, directly irradiated vortex flow and indirectly irradiated entrained flow reactors. Packed bed reactors are robust but heat and mass transfer are limited even if the residence time is long. Vortex flow and entrained flow reactors show improved heat and mass transfer but the feedstock size is limited. Direct irradiation enables better heat transfer to the reactants but the challenge is to avoid any dirt on the window. The solar spouted bed reactor has recently been proposed (Boujjat et al., 2019). It can operate either in direct or indirect heating modes. Heat and mass transfer are enhanced by the gas jet that stirs the particles injected continuously in the reactor. Various types of feedstock can be treated as the solid residence time is long.

Wood biomass (overall formula can be assumed as $C_6H_9O_4$) can be commonly gasified either with steam or CO_2 (Billaud et al., 2016).

Steam gasification:

$$C_6H_9O_4 + 2H_2O \rightarrow 6.5H_2 + 6CO\ \Delta H^\circ = 800\text{kJ/mol} \quad (1)$$

CO_2 (dry) gasification:

$$C_6H_9O_4 + 2CO_2 \rightarrow 4.5H_2 + 8CO\ \Delta H^\circ = 883\text{kJ/mol} \quad (2)$$

Chemical looping can also be considered. Such process is a relatively old concept initially proposed for CO_2 separation in combustion. Then, it was applied to gasification, reforming, and more recently to chemical looping hydrogen production (Zhao et al., 2017). The objective of chemical looping gasification is to rely on a low-cost oxygen source and self-heating system, while producing high quality syngas. Iron oxide is one of the most studied solid oxygen carriers (Yu et al., 2019) while the concept of liquid chemical looping has only recently been proposed (Sarafraz et al., 2017a,b). It offers the major advantages of being a low-cost material with no environmental impact. Various types of carbonaceous feedstocks have been investigated. Wu et al. suggested to study the kinetics using cellulose as the main organic component of biomass (Wu et al., 2019). The main reported works used electric furnaces (Huang et al., 2014), or thermogravimetric analysis (Huang et al., 2015; Zeng et al., 2018) with a heating rate of about 10°C/min. A systematic review proposed by Gauthier et al. (2013) highlights a particular need to use experimental setups for which heating conditions are controlled (imposed temperature or heat flux). When using solar energy, it is possible to supply high-temperature solar heat to the gasifier and the air reactor (oxidation step) can be replaced by a water or CO_2 splitting reactor to produce additional syngas (Krenzke et al., 2017). This splitting method was proposed in the steam-iron process that uses syngas (or carbonaceous feedstocks) to reduce iron oxide. The reduced form of iron oxide is then re-oxidized with steam to form hydrogen and magnetite (Hacker et al., 2000). Solar-driven extractive metallurgy has also been investigated (Fernández-González et al., 2018). Solar chemical looping biomass gasification has only been explored over zinc oxide, zinc product being a volatile material (Chuayboon et al., 2018). In this work, the biomass gasification over iron oxide (non-volatile material) in an induction furnace was investigated. The objective was to compare biomass reactivity under high heating rates similar to the ones achieved in solar reactors (500°C/s) with different oxidizing agents (iron oxide, H_2O or CO_2). The overall endothermic reaction is:

$$C_6H_9O_4 + 2/3Fe_2O_3 \rightarrow 4/3Fe + 6CO + 4.5H_2\ \Delta H^\circ = 865\text{kJ/mol} \quad (3)$$

First, the biomass pyrolysis occurs leading to syngas, tars and char (carbon). Char can be further gasified by iron oxide. The Fe_2O_3 carbothermal reduction steps are as follows:

$$C + 3Fe_2O_3 \rightarrow 2Fe_3O_4 + CO\ \Delta H^\circ = 121.6\text{kJ/mol} \quad (4)$$

$$C + Fe_3O_4 \rightarrow 3FeO + CO\ \Delta H^\circ = 207.1\text{kJ/mol} \quad (5)$$

$$C + FeO \rightarrow Fe + CO\ \Delta H^\circ = 156\text{kJ/mol} \quad (6)$$

Pyrolysis gases undergo subsequent reactions including mainly reforming and water-gas shift reactions (Dupont et al., 2007).

Since metallic Fe can be obtained, the process could support the energy transition in the metallurgical industry whose conventional processing is releasing large amounts of CO_2 in the atmosphere due to the extensive use of fossil resources (accounting for 6% of anthropogenic CO_2 emissions) (IEAGHG, 2013).

In addition, Fe can also be converted back to Fe_3O_4 by water oxidation producing hydrogen while Fe_3O_4 can be oxidized to Fe_2O_3 only with oxygen (Yang et al., 2008). The exothermic oxidation reactions can be written as:

$$Fe + 4/3H_2O \rightarrow 1/3Fe_3O_4 + 4/3H_2\ \Delta H^\circ = -50\text{kJ/mol} \quad (7)$$

$$Fe_3O_4 + 1/4O_2 \rightarrow 3/2Fe_2O_3\ \Delta H^\circ = -116\text{kJ/mol} \quad (8)$$

This last step could be an option to ensure heat supply for continuous biomass conversion at night or during transient periods with low solar power input in the case of a solar chemical looping gasification process [thermochemical heat storage (André et al., 2018)].

In this study, thermodynamic equilibrium calculations were first performed in order to determine the chemical species involved in the case of biomass gasification with H_2O, CO_2, and iron oxide. Then, the experimental equipment and procedure were described and the results were analyzed and compared for the three oxidizing agents.

THERMODYNAMIC EQUILIBRIUMS

Method

Thermodynamic equilibriums were calculated using Gibbs free energy minimization (GEMINI2 software) (Cheynet and

Chevalier, 2002). This approach uses databases containing the standard Gibbs energy of the most common molecules. The overall formula of beech wood was considered as $C_6H_9O_4$ based on its global chemical composition. Most thermodynamic properties of gases and the different iron oxides are available in this database but there is no data for any kind of solid biomass feedstock. Thus, biomass was included into the model in the form of dioxygen, dihydrogen, and solid carbon. This model presents several advantages as it does not require to know the different reactional mechanisms and can be applied to any reactor geometry. Furthermore, it is possible to change the temperature and pressure conditions to study their impact on the composition of the mix at the equilibrium state. The equilibrium results are thermodynamic predictions for a closed system that do not take into account any kinetic aspect, especially the reactants residence time but also reaction site deactivation, sintering, and agglomeration. Anyway, this is a first approach to determine the theoretical limit of the conversion process and to identify expected products.

In the case of thermodynamic equilibrium studies, the reactants are often introduced in stoichiometric proportion which is not the case in a real gasification process. To ensure an optimal reaction rate with biomass in a real process, the oxidizing agent is often introduced in over-stoichiometric proportion. Thus, thermodynamic equilibriums were calculated with both stoichiometric and over-stoichiometric proportions of oxidizing agent in order to study the impact on the products composition. For each situation, the calculations were realized at temperatures ranging from 100°C to 1,500°C every 50°C at atmospheric pressure. The results relate to the quantity of the main gases (H_2, CO, CO_2, CH_4, and H_2O) produced per gram of gasified dried biomass along with the LHV (Low Heating Value) of the produced gas mix (CO, H_2, and CH_4). The other predicted gas species, such as hydrocarbons (C_2H_4, C_2H_6), appearing in very low amounts ($<10^{-5}$ mmol/$g_{biomass}$) are not presented and are neglected. Calculations in over-stoichiometric proportion of oxidizing agent (H_2O, CO_2, Fe_2O_3) were realized with twice and three times the stoichiometric amount of oxidizing agent. Even though the results were slightly different, the obtained tendencies are similar and thus only the results of the calculations with three times the stoichiometric proportion of oxidizing agent will be presented.

Water as Oxidizing Agent

The gas species produced from steam biomass gasification in stoichiometric and over-stoichiometric proportions are presented in **Figure 1**.

Concerning the results in stoichiometric proportion, CH_4 and CO_2 productions are predominant compared to CO and H_2 below 450°C. With the increase of the H_2 production starting at 250°C, a decline of the CH_4 produced occurs (as well as the remaining water). The quantity of produced CO_2 rises steadily until reaching a peak at 550°C and then decreases to become insignificant above 900°C. All the carbon of the original biomass is found in the form of CO above 900°C. The equation (**1**) completion is reached from 900°C and products remain stable at higher temperatures (the gas mix LHV is then 23.39 MJ/$kg_{biomass}$). As a comparison, the LHV of a typical dry wood biomass is 18 MJ/kg, which demonstrates the upgrade of the calorific value of the feedstock. These results are in agreement with those reported for the gasification of cellulose (Hathaway et al., 2014) and carbon (Gokon et al., 2015), the main difference being the higher production of H_2 due to the higher quantities of hydrogen contained in the presently selected biomass.

When steam is present in over-stoichiometric proportion, the production of CO_2 is higher and is responsible for a lower production of CO. Even though the production of CO_2 starts decreasing at higher temperatures, CO_2 is still present at 1,500°C. The production of H_2 is also higher at any given temperature. The LHV of the gas mix at high temperature (maximum of 23.09 MJ/$kg_{biomass}$ at 1,500°C) is slightly lower than the one in stoichiometric proportion.

CO_2 as Oxidizing Agent

Figure 2 displays the equilibrium composition for biomass gasification with stoichiometric and over-stoichiometric CO_2 proportion (Equation 2).

As expected, the quantity of CO produced from gasification with CO_2 is higher than with steam gasification whereas the H_2 quantity is lower. The completion of Equation (2) is only reached above 1,000°C due to the fact that the Boudouard equilibrium ($C+CO_2 \leftrightarrow 2CO$) requires such high temperatures for a complete gasification. CO and H_2 are produced in low quantity at low temperature and CH_4 is produced in lower quantity compared to steam gasification. However, water is produced below 900°C. The LHV reaches a maximum value of 24.29 MJ/$kg_{biomass}$ which is slightly higher than the maximum LHV obtained with steam.

Similar to steam, calculations with CO_2 in over-stoichiometric proportion do not reach reaction completion at high temperature. After reaching a minimum at 700°C the production of water increases with the temperature. At this temperature, the production of CO also exceeds the one reached at the theoretical equilibrium in **Figure 2A** (55.1 mmol/$g_{biomass}$) and the H_2 production decreases. This evolution is due to the reverse water-gas shift reaction ($CO_2 + H_2 \rightarrow CO + H_2O$). The LHV increases very slowly from 750°C to 1,500°C and reaches a maximum of 25.16 MJ/$kg_{biomass}$ at 1,500°C.

Iron Oxide as Oxidizing Agent

Figure 3 illustrates the thermodynamic equilibria when using iron oxide as the oxidizing agent (Equation 3) either in stoichiometric proportion or in excess.

In stoichiometric proportion, the theoretical reaction completion is reached at 1,000°C and above (at these temperatures, the syngas LHV is 20 MJ/$kg_{biomass}$). It is noticeable that the production of CO is the same as with steam gasification and the production of H_2 is the same as with CO_2 gasification in accordance with reactions (**1**), (**2**), and (**3**). When iron oxide is introduced in over-stoichiometric proportion, the additional oxygen provided to the system results in the production of CO_2 at high temperature to the detriment of the CO production and syngas LHV. The CO_2 also reacts with the H_2 to produce H_2O (reverse water-gas shift reaction). This reaction is favored at higher temperature when the production of H_2O becomes more

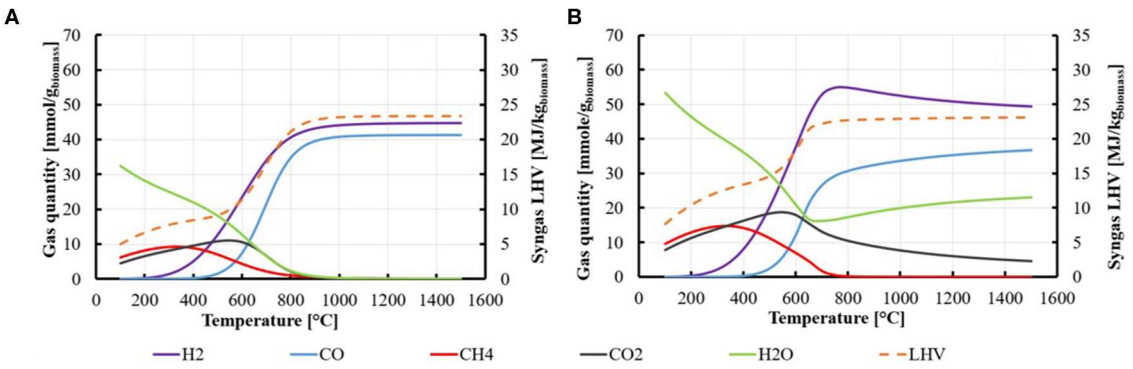

FIGURE 1 | Quantity of gases produced at thermodynamic equilibrium per gram of dry biomass from steam gasification of wood according to temperature: **(A)** stoichiometric proportion $\mathbf{C_6H_9O_4+2H_2O}$; **(B)** over-stoichiometric proportion $\mathbf{C_6H_9O_4+6H_2O}$.

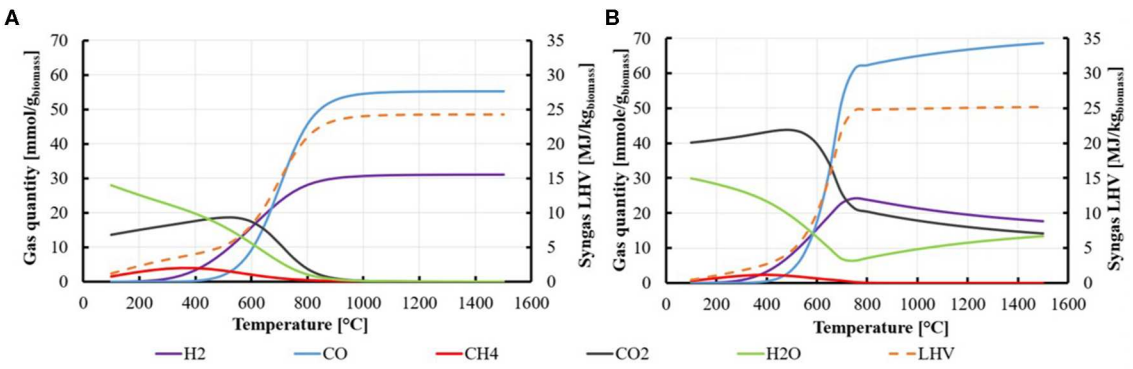

FIGURE 2 | Quantity of gases produced at thermodynamic equilibrium per gram of dry biomass from gasification of wood with carbon dioxide according to temperature: **(A)** stoichiometric proportion $\mathbf{C_6H_9O_4+2CO_2}$; **(B)** over-stoichiometric proportion $\mathbf{C_6H_9O_4+6CO_2}$.

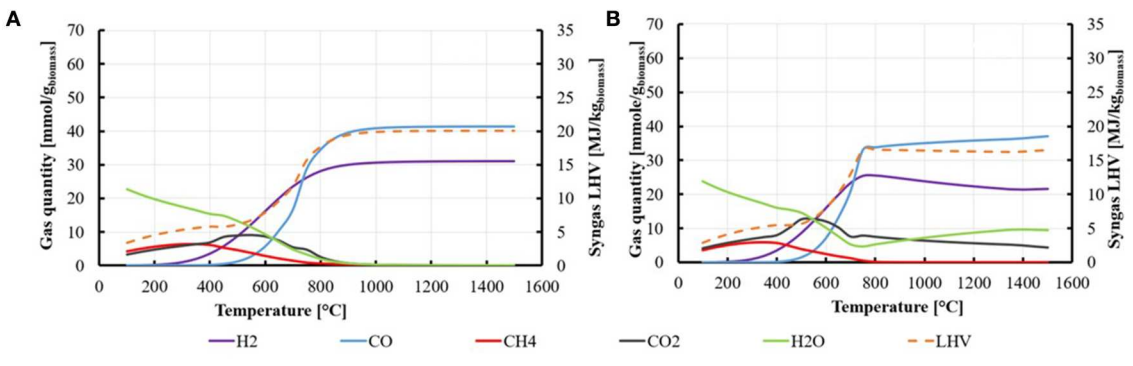

FIGURE 3 | Quantity of gases produced at thermodynamic equilibrium per gram of dry biomass from gasification of wood with iron oxide according to temperature: **(A)** stoichiometric proportion $\mathbf{C_6H_9O_4+\frac{2}{3}Fe_2O_3}$; **(B)** over-stoichiometric proportion $\mathbf{C_6H_9O_4+2Fe_2O_3}$.

significant. **Figure 4** plots the quantities of iron species (Fe_2O_3, Fe_3O_4, FeO, Fe) obtained at thermodynamic equilibrium for stoichiometric gasification conditions over iron oxide. Metallic iron (Fe) can be obtained for temperatures beyond 750°C in the presence of biomass as reducing agent, whereas the direct thermo-reduction of iron oxide requires much higher temperatures (Charvin et al., 2007).

All the thermodynamic calculations reveal that the gasification reaction should be carried out at temperatures beyond 1,000°C to maximize the biomass conversion. Thus, experiments were

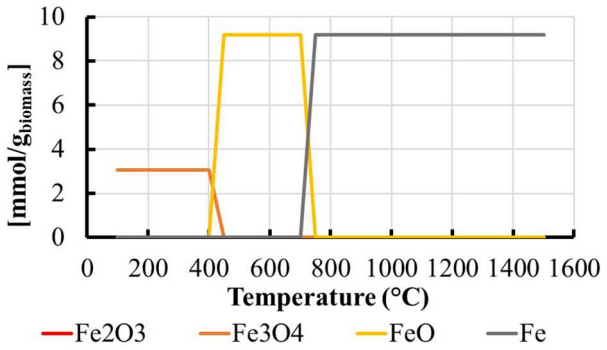

FIGURE 4 | Quantity of iron species obtained at thermodynamic equilibrium per gram of dry biomass from gasification of wood with iron oxide in stoichiometric proportion ($C_6H_9O_4 + \frac{2}{3}Fe_2O_3$) according to temperature.

performed at 1,100°C to provide additional information about the kinetics and gas products composition.

EXPERIMENTAL SECTION

Feedstock

The biomass used for the experiments consisted of beech wood particles whose characteristics are given in **Table 1**. They were obtained from XP CEN/TS 15104, XP CEN/TS 15105, XP CEN/TS 15107, XP CEN/TS 14775 standards. Oxygen content was deduced by difference. The LHV (dry basis) was measured with a PARR 6200 bomb calorimeter knowing humidity from NF EN 14774 standard. Granulometry was obtained using a FT4 granulometer. The biomass was first dried at 105°C overnight and then kept under vacuum to avoid humidity in the samples.

Regarding iron oxide, a fine powder of ferric oxide was used (iron oxide (III), Fe_2O_3, purity > 99.5%, size < 5 μm). This powder size allowed for an easy mix with the biomass particles with uniform coating at the biomass surface providing a good solid to solid contact. During the preparation of each sample, iron oxide was mixed with biomass in the desired proportion and a 3g sample of the mix was placed in the sample holder. The sample holder was then introduced in the Inconel tube of the experimental bench and a nitrogen flow was injected to prevent the humidification of the sample.

Experimental Setup

The PYRATES experimental bench was designed for fast pyrolysis and gasification of small samples using an induction furnace that allows for fast heating rates (500°C/s) (Gauthier et al., 2013). The experimental bench and its components are described in **Figure 5**.

The 12 kW induction batch furnace (HFP 12, EFRD induction Gmbh) heated an Inconel 600 pipe (33.5 mm diameter) with a four-coil inductor (6 cm height). The temperature at the surface of the Inconel pipe was measured and regulated with a two-color pyrometer (IMPAC infratherm, range 350–1,300°C, λ_1 =1.52 μm, λ_2 =1.64 μm, response time 2 ms, precision is +/-(0,4%.T+1)) between the two central coils. A quartz pipe provided the sealing of the furnace. A porous metallic sample carrier enabled the gas passage through the biomass particles. A 50°C temperature difference was observed between the wall temperature and the sample after 4 min heating (Gauthier et al., 2013). The evaluation of the sample temperature is considered as the main experimental uncertainty. In the following, as no temperature measurement inside the sample exists, the sample temperature (T_{wall}-50°C) was taken as reference. During the heating period, a N_2 flow of 2 NL/min [NL means Normal Liter at normal temperature (0°C) and pressure (101,325 Pa)] was maintained at the bottom of the Inconel tube to avoid biomass humidification with ambient air. Gaseous oxidizing agents were injected from the bottom. An additional flow of nitrogen (3 NL/min) was used at the hot zone exit for gas quenching and condensation of condensable gases. These gases condensed on the quartz tube wall (**Figure 5**, marker 6) while a collector (**Figure 5**, marker 7) enabled tar recovery if large quantities were produced. The off gases passed through an electrostatic precipitator, a serpentine ice trap (0°C), two washing bottles inserted in a dry ice and isopropanol bath (−70°C) and then a cartridge filter to retain all condensable gases before analysis.

Metrology and Gas Analysis

Gas composition was analyzed continuously using a mass spectrometer and a Fourier Transform InfraRed (FTIR) spectrometer. A gas flow of 1 NL/min was extracted after its passage through the cartridge filter to be analyzed by the mass spectrometer (Adixen ASM1025) measuring only the H_2 concentration with a 1 s measurement interval. The rest of the gas flow was directed toward the FTIR spectrometer (Nicolet IR 550) that continuously measured the concentrations of CO, CO_2, CH_4, C_2H_4, C_2H_2, CH_3OH, and H_2O. The gas was then stored in a sampling bag (**Figure 5**, marker 13) to be analyzed after the end of the experiment with a four columns gas-phase micro-chromatograph (Agilent 3000A). The columns A and B (molecular sieve 5 Å, 10m) had a 90°C inlet temperature and used, respectively, argon and helium as carrier gas. Column C (PPU, 8m) and Column D (CP wax 52, 10m) had an inlet temperature of 80°C and 40°C, respectively, and both used helium as carrier gas. The micro-chromatograph was used for the measurement of the concentration of CO, CO_2, CH_4, C_2H_4, H_2, C_2H_6, C_3H_8, C_2H_2, C_6H_6, and C_7H_8. A 13% discrepancy was evaluated on gas mass, based on comparisons between FTIR continuous analysis and micro-chromatograph measurements (the latter being taken as reference).

RESULTS AND DISCUSSION

Effect of Oxidizing Agent

In order to evaluate the relevance of the biomass gasification over iron oxide, a comparison with pyrolysis along with CO_2 and H_2O gasification was performed. Four runs were carried out at 1,100°C for 20 min with a total bottom gas flow of 1 NL/min to maintain same space times between runs. The pyrolysis run was carried out with 1 NL/min of N_2. In the case of H_2O and CO_2, oxidant injection was continuous. Pure CO_2 (1 NL/min) was injected for CO_2 gasification (about 20

TABLE 1 | Ultimate composition and characteristics of the biomass used in the experiments.

Composition						LHV (MJ/kg)	Mean particle size (mm)
C (w%)	H (w%)	O (w%)	N (w%)	S (w%)	Ashes (w%)		
52.8	7.1	40.7	0.14	<0.1	0.29	18.3	0.3

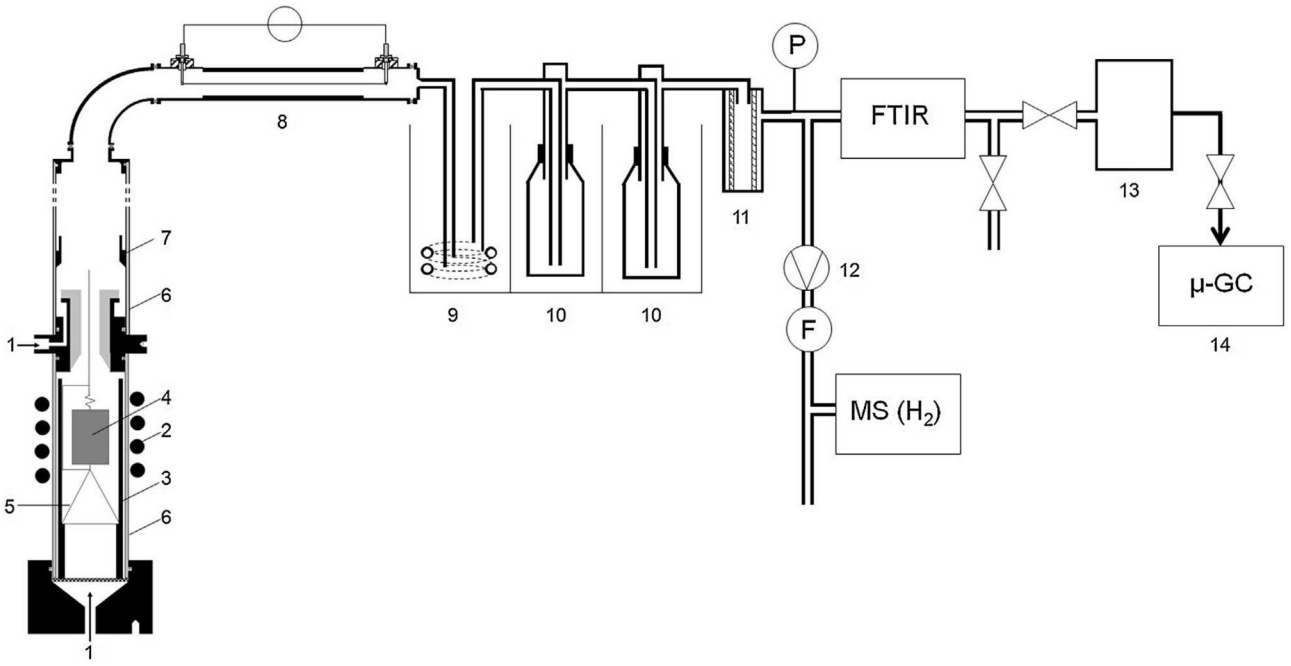

FIGURE 5 | Experimental bench PYRATES : (1) Gas inlet (N_2 on top, N_2, CO_2 and H_2O on bottom); (2) Inductor; (3) Inconel pipe; (4) Wood sample; (5) Metallic sample holder; (6) Quartz pipe; (7) Tar collector; (8) Electrostatic precipitator; (9) Ice trap (0°C); (10) Dry ice trap (−70°C); (11) Cartridge filter; (12) Pump; (13) Tedlar bag; (14) Micro-Gas chromatograph; (FTIR) Fourier Transform InfraRed Spectroscope; (MS) Mass spectroscope (Gauthier et al., 2013).

times the stoichiometry over the run period). For H_2O, N_2 was required to limit condensation and thus a mixture of 20% of water and 80% of nitrogen (in volume) with a H_2O flowrate of 0.2 NL/min was injected (corresponding to about 4 times the oxidant stoichiometry over the run period). Finally, a mass fraction of iron oxide of 70% was set in the initial sample for solid-solid gasification (about 2 times the stoichiometry) along with a continuous N_2 flow (1 NL/min). In all cases, the oxidizing agent was in excess even if not in the same proportion; quantitative results and qualitative comparison are commented for each case. **Table 2** reports the gas yields and syngas LHV for the four runs. They were obtained from the gas analysis system giving the various concentrations while N_2 tracer gas method was used to determine the total flowrate. LHV was calculated from the given gas composition. All quantities are reported with respect to the initial mass of biomass. The total gas productions (H_2, CO, CO_2, CH_4, and C_2H_4) are reported in **Figure 6** while **Figure 7** shows the online concentrations of H_2, CO, CO_2, CH_4 over the run duration (20 min). The productions are compared for the various oxidizing agents (H_2O, CO_2, Fe_2O_3) and for pyrolysis. CO_2 production is not reported in the case of CO_2 gasification as it comes not only from the gasification reaction but also from the CO_2 feed.

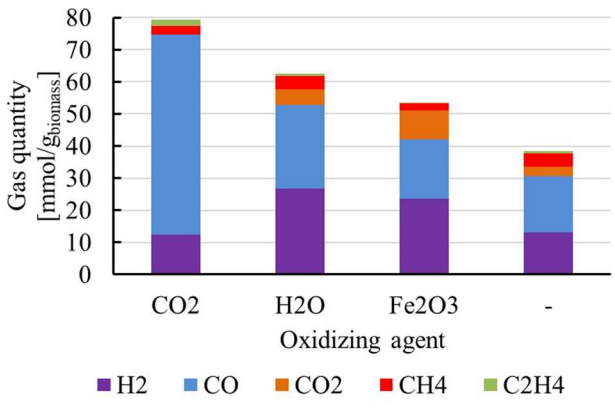

FIGURE 6 | Quantities of gases produced during gasification at 1,100°C with CO_2, H_2O, Fe_2O_3 and without oxidizing agent (pyrolysis).

Results were compliant with the trends observed from thermodynamic calculations. H_2 production was maximum for steam gasification while CO_2 gasification showed the highest amounts of CO. The gas production was lower with iron oxide

TABLE 2 | Total gas quantities produced during gasification and pyrolysis at 1,100°C.

Oxidizing agent	Gas production [mmol/$g_{biomass}$]									LHV (MJ/$kg_{biomass}$)
	H_2	CO	CO_2	CH_4	C_2H_4	C_2H_2	CH_3OH	H_2O	Total	
CO_2	9.93	51.58	–	3.33	0.26	0.08	0.04	0.28	65.50	21.27
H_2O	26.64	26.26	4.76	4.24	0.65	0.09	0.02	–	62.66	18.8
Fe_2O_3	23.49	18.61	9.07	2.10	0.01	0.02	0.02	0.32	53.64	13.06
None (pyrolysis)	13.12	17.54	2.93	4.16	0.58	0.08	0.02	0.18	38.60	12.72

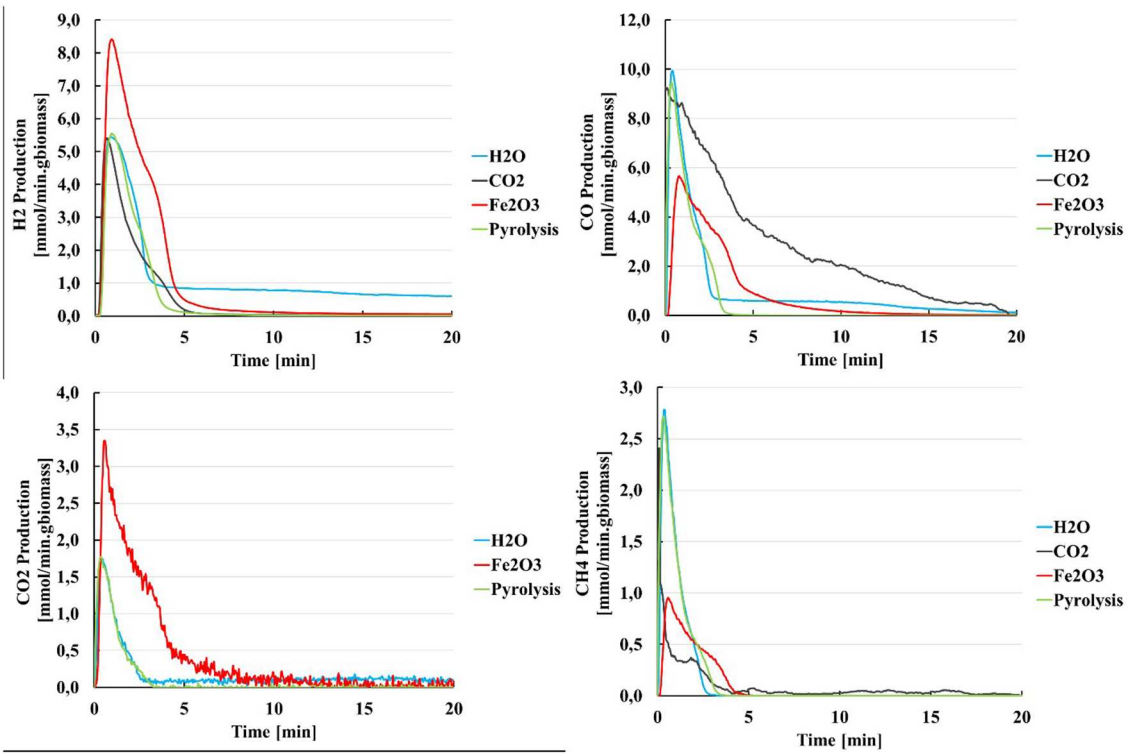

FIGURE 7 | Evolution of the gas production during gasification with CO_2, H_2O, and Fe_2O_3 and pyrolysis of the batch of biomass.

than with other oxidants but still higher than during the pyrolysis run (no oxidizing agent).

Interestingly, for the pyrolysis run, all gases were produced in < 4 min. Thus, for the other runs, any gas production occurring after 4 min should be the result of the char gasification reaction.

Concerning H_2, the production was very similar during the first 4 min for the runs with water, CO_2 or without oxidant. The peak production was about 5.5 mmol/min.$g_{biomass}$. After 5 min, a weak H_2 production was maintained only for water as oxidizing agent, which came from the char gasification with water that also produced CO and CO_2. For the gasification over iron oxide, the H_2 production was much more pronounced with a peak production at 8.35 mmol/min.$g_{biomass}$ for a total duration of 5 min. However, the total H_2 production from steam gasification was higher but with a lower kinetic.

CO production was maximum for CO_2 gasification but the total produced quantity (51.6 mmol/$g_{biomass}$) was still well-below the equilibrium value (65.9 mmol/$g_{biomass}$). The first minutes of CO production were very similar between steam gasification and pyrolysis but steam gasification maintained a CO production after 3 min due to progressive char gasification which was not possible without oxidant (pyrolysis). CO production from pyrolysis stopped after 4 min while CO production from steam gasification only slowly decreased after 3 min. Gasification with iron oxide showed a lower CO peak production than the other cases with a total production barely exceeding that of pyrolysis. This result is mainly to be linked with the high production of CO_2 over iron oxide (two to three times the total amount obtained for water gasification and pyrolysis). This could come from the reaction of iron oxide with char ($2Fe_2O_3 + 3C \rightarrow 4Fe + 3CO_2$). The high availability of oxygen from Fe_2O_3 was also reported in chemical looping methane reforming, leading also to a CO_2 production peak during the first cycle (Chuayboon et al., 2019).

Concerning CH_4, the gas production occurred during the first 4 min of all runs as methane was produced during the pyrolysis step. Steam gasification and pyrolysis resulted in the highest methane production peak (2.8 mmol/min.$g_{biomass}$). For pyrolysis, the large amount of CH_4 is explained by the fact that steam reforming reaction cannot occur (no water injection) while for steam gasification, the short residence time tends to hinder gas phase reactions. The lowest methane production was obtained for the gasification run over iron oxide. Indeed, reduced iron oxide has shown high selectivity toward H_2 and CO in dry reforming (Zhu et al., 2019). This last reaction is favored by the relatively high CO_2 concentration obtained with iron oxide.

As for methane, C_2H_4 and C_2H_2 productions were minimal for gasification over iron oxide. Methanol production remained very small in all cases.

Concerning the LHV of the products, CO_2 and H_2O gasification produced a syngas containing more energy than the initial biomass (18.3 MJ/kg). Solar gasification is a way to upgrade the heating value of the biomass. The Cold Gas Efficiency (CGE) permits to quantify this upgrade. This efficiency is not an energy efficiency and is sometimes called energy Upgrade Factor (F_U) in the field of solar reactors (Zgraggen and Steinfeld, 2008):

$$F_U = \frac{LHV_{syngas} * m_{gas}}{LHV_{biomass} * m_{biomass}} \quad (9)$$

F_U superior to 1 means that the produced syngas offers a higher energy content than the initial feedstock. For CO_2 gasification, the F_U is 1.16; it is 1.03 for steam gasification while the F_U for pyrolysis is 0.7. Taking into account only the reduction step, the F_U of the gasification over iron oxide is comparable to pyrolysis (0.71). However, the hydrogen produced through the re-oxidation step should be added (not quantified experimentally) and F_U superior to one are theoretically achievable.

These results provide qualitative information about the use of iron oxide as oxygen carrier for the gasification reaction (solid-solid reaction) vs. more common solid-gas reactions (steam and dry gasification). The comparison between the two systems (solid-solid and gas-solid) is not obvious because chemical mechanisms are different but the same reactor was used. Especially, the high reactivity observed with iron oxide may be due to the fact that the oxidizing agent is already mixed with the biomass at the beginning of the run, while H_2O and CO_2 have to penetrate the biomass sample. Also, the experimental device is mainly dedicated to the pyrolysis study as the gas residence time in the heated zone is short. Anyway, the feasibility of the solid-solid reaction is demonstrated and it shows promising performance that can possibly be enhanced with continuous particles stirring. Additionally, the effect of the iron oxide proportion in the initial biomass feedstock was studied.

Influence of the Iron Oxide Stoichiometry

The influence of the proportion of iron oxide (in default, stoichiometric, excess) was studied for a mass fraction of 0.25 (oxide in default), 0.5 (stoichiometric proportion), and 0.66 (oxide in excess). A run without oxide (pyrolysis) was also carried out. Samples were heated up to 1,050°C for 10 min. The main conditions and results (initial and final sample masses, gas yield, syngas LHV, carbon conversion) are recapped in **Table 3**. Carbon conversion is defined as:

$$X_C = \frac{m_{C_{syngas}}}{m_{C_{biomass}}} \quad (10)$$

Where $m_{Csyngas}$ is the mass of carbon contained in the syngas and $m_{Cbiomass}$ the mass of carbon in the initial biomass.

For better readability, **Figure 8** plots the H_2, CO, CO_2, and CH_4 yields along with the syngas LHV as a function of iron oxide initial mass fraction in the sample. Concerning the initial and final masses of the samples, when iron oxide mass fraction was 0.5 or 0.66, the final mass of the sample was lower than the initial oxide mass. This proves that oxygen was transferred from

TABLE 3 | Gas yields through gasification of biomass with Fe_2O_3 at 1,050°C as a function of the oxidant mass fraction.

Fe_2O_3 mass fraction		0	0.25	0.5	0.66
Sample initial mass (g)		3.184	2.658	3.04	3.168
Sample final mass(g)		0.504	1.173	0.913	1.823
Tar mass (g/$g_{biomass}$)		0.211	0.14	0.233	0.176
Gas yield (mmol/$g_{biomass}$)	H_2	18.716	23.043	25.878	29.584
	CO	12.997	11.210	15.110	16.084
	CO_2	3.639	5.813	8.163	10.180
	CH_4	4.011	2.560	2.431	1.534
	H_2O	0.362	0.082	0.310	0.048
	C_2H_4	1.111	0.743	0.558	0.379
	C_2H_6	0.061	0.022	0.009	0.005
	C_2H_2	0.312	0.282	0.188	0.169
	C_3H_8	0.055	0.020	0.000	0.000
	Toluene	0.000	0.088	0.077	0.084
	Methanol	0.133	0.023	0.013	0.009
	Benzene	0.000	0.088	0.077	0.084
Syngas LHV (MJ/$kg_{biomass}$)		13.82	13.04	14.30	14.55
Carbon conversion rate		55.08%	52.76%	65.03%	69.11%

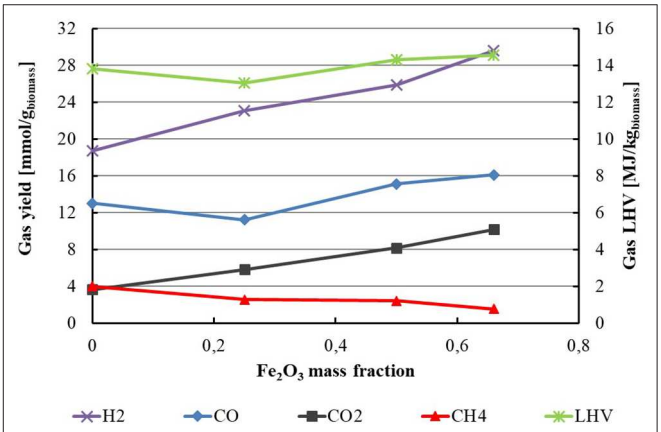

FIGURE 8 | Gas yield at 1,050°C and LHV of the produced gas according to the Fe_2O_3 mass fraction.

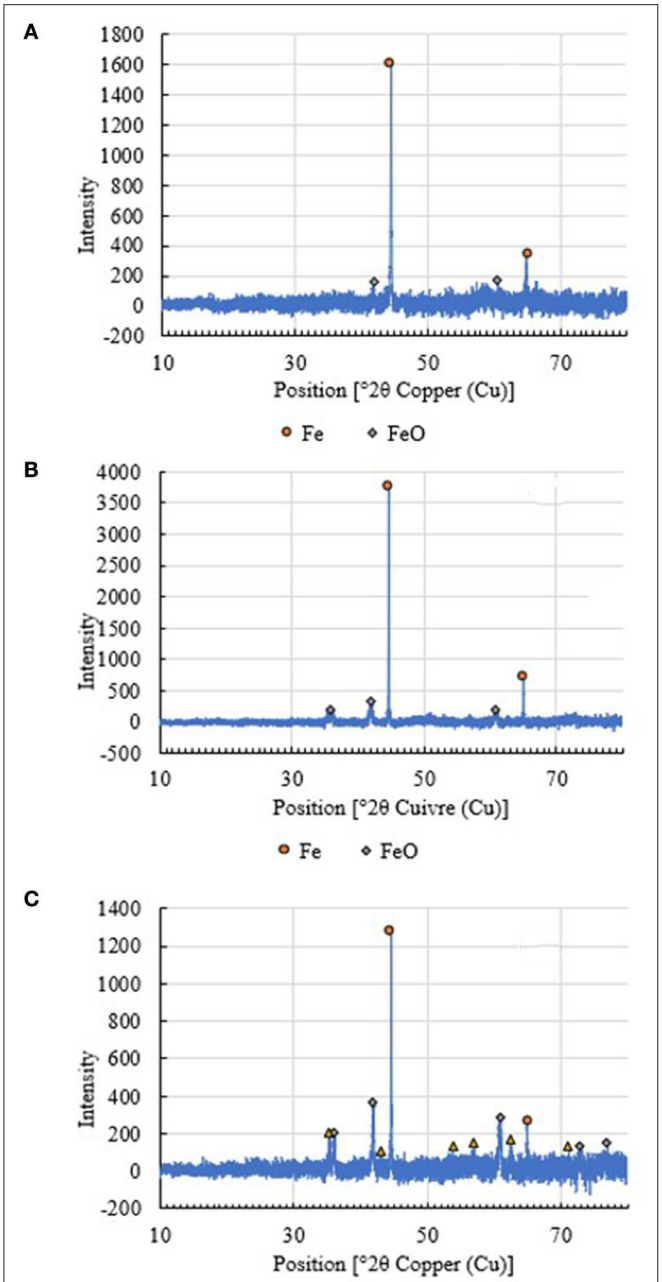

FIGURE 9 | Diffractograms of the solid products from biomass gasification with iron oxide: **(A)** 75w% biomass and 25w% iron oxide, **(B)** 50w% biomass, and 50w% iron oxide, **(C)** 34w% biomass and 66w% iron oxide.

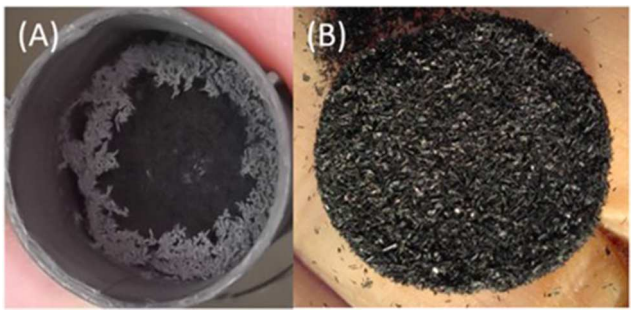

FIGURE 10 | Solid residue after biomass gasification over iron oxide (25w%): **(A)** sample holder containing the residue **(B)**: char and reduced iron oxides pellets recovered at the bottom of the sample holder.

the oxide to the biomass for the gasification reaction. Conversely, when the iron oxide mass fraction was 0.25, the final mass of the sample (containing unreacted char and iron oxide) was higher than the initial mass of iron oxide denoting a limited reaction extent. The mass fraction of iron oxide had a significant impact on the gas yield. H_2 and CO_2 yields increased clearly (from 18.7 to 29.6 mmol/$g_{biomass}$ and 3.6 to 10.2 mmol/$g_{biomass}$, respectively) while CH_4 yield decreased (from 4.0 to 1.5 mmol/$g_{biomass}$) with the increase of the iron oxide mass fraction. The CO yield showed a minimum of 11.2 mmol/$g_{biomass}$ for an oxide mass fraction of 0.25. The impact on the syngas LHV was finally limited as the minimum value was 13 MJ/$kg_{biomass}$ and the maximum value was 14.5 MJ/$kg_{biomass}$. Noteworthy, the excess of iron oxide did not reduce the syngas LHV as predicted by the thermodynamic equilibrium calculations and the syngas LHV always remained lower than the biomass LHV of 18 MJ/kg. This is to be linked to the low carbon conversion obtained (maximum of 70% for an iron oxide mass fraction of 0.66). While the H_2 yield was close to the theoretical values (25.9 vs. 30 mmol/$g_{biomass}$ for a stoichiometric blend), the CO yield differed from the calculations (15.1 vs. 42 mmol/$g_{biomass}$ for a stoichiometric blend). This was also true for the CO_2 yield (8.2 mmol/$g_{biomass}$ while no CO_2 is predicted by the thermodynamic calculations). Since gas phase reactions were minimized in the experiment (low gas residence time), it is expected that dry reforming reaction ($CH_4 + CO_2 \rightarrow 2CO + 2H_2$) is not favored. Also, the excess of oxygen carrier can lead to partial combustion of chars and thus to additional CO_2 production.

X-ray Diffraction analysis (XRD, Panalytical X'PERT PRO, Cu Kα radiation, αCu = 0.15418 nm, angle range = 10–80°, 2theta) was performed to identify the phase composition of the final solid products. The identification of the crystalline phases was realized by peak indexation and comparison with reference compounds giving standard diffraction peaks (powder diffraction file PDF-2, International Center for Diffraction Data, ICDD). For each run of **Table 3**, XRD diffractograms are given in **Figure 9**. Diffraction peak corresponding to metallic iron (JCPDS n° 00-001-1262) or to iron oxides (FeO, JCPDS n° 00-002-1180; Fe_3O_4, JCPDS n° 00-001-1111; Fe_2O_3 JCPDS n° 00-024-0072) were identified. For the iron oxide mass fraction of 25% (biomass in excess) (**Figure 9A**), Fe was mainly identified with some traces of FeO. This proves that iron oxide was almost totally reduced and thus that particle-particle contacting was effective for an excess of biomass. Given the fact that the proportion of iron oxide was lower than the one required for complete gasification, a total iron oxide reduction was expected and experimentally confirmed. A corresponding low carbon efficiency was obtained (53%) due to the lack of oxidant species. For an oxide mass fraction of 0.5

(**Figure 9B**), metallic Fe was still the dominant specie in the sample which could again be expected from a stoichiometric blend. Some traces of FeO were also identified. The carbon conversion increased to 65%. Finally, for the highest iron oxide mass fraction (excess of iron oxide, **Figure 9C**), no trace of Fe_2O_3 was found but Fe, FeO, and Fe_3O_4 were present with Fe as the main specie. Indeed, as iron oxide was in excess with respect to reaction stoichiometry, total iron oxide reduction into Fe was not possible. Even if all Fe_2O_3 particles reacted with the biomass, the impact on the carbon conversion was limited as it reached 69%. During the initial reaction steps, the solid-solid reaction was efficient as a result of good contact between micrometric iron oxide particles and millimetric biomass particles (with the oxide particles spread at the surface of the biomass particles). However, the particles were static and during the reaction progress the contact between particles was progressively reduced leading to limited mass transfer and thus limited carbon conversion rate. **Figure 10** shows that the iron and iron oxides particles remaining in the sample holder kept the shape of their surrounding biomass particles on which they were in contact before gasification. Even if a large part of the biomass was gasified, it is possible to distinguish small gray heaps mainly composed of metallic iron which corresponded initially to biomass particles covered by iron oxide. This structure was mainly visible at the top of the sample holder (**Figure 10A**). The remaining solid residue (char+iron oxide) collapsed at the bottom of the sample holder in the form of a dark gray pellet (**Figure 10B**). These observations highlight the need for stirring the particles to enhance mass transfer, carbon conversion and ultimately LHV of the syngas.

CONCLUSION

This study focused on the combined biomass gasification and iron oxide reduction for both syngas and iron production. This process can be coupled with concentrated solar energy for renewable fuel production and green iron metallurgy. Original results about beech wood biomass gasification over iron oxide (Fe_2O_3), H_2O, and CO_2 were reported. First, a theoretical study was carried out about the thermodynamic equilibrium calculations associated with the different chemical systems depending on the temperature and mass ratio of oxidizing agent. Then, the feasibility of the process was proven in an induction furnace able to reproduce high heating rates representative of concentrating solar installations. Iron oxide was successfully reduced to metallic iron at temperature above 1,000°C concomitantly with the production of hydrogen-rich syngas. A low carbon conversion (<70%) was observed because of mass transfer limitation in the developed fixed bed reactor. The results were compared with dry and steam biomass gasification along with pyrolysis in order to emphasize the remarkable performance obtained with a solid-solid gasification system involving iron oxide as oxygen carrier. In addition, when coupled with concentrated solar energy for supplying process heat, the solar gasification over iron oxide can produce green iron in a sustainable metallurgical process or additional hydrogen via chemical looping in a steam-iron process. Future work should focus on continuous biomass gasification with iron oxide under concentrated solar radiation to demonstrate the feasibility of the novel metallurgical process for high-purity syngas and Fe production. Such a solar process will represent a new promising renewable path toward sustainable solar fuels and chemical commodities.

DATA AVAILABILITY STATEMENT

The original contributions presented in the study are included in the article/supplementary materials, further inquiries can be directed to the corresponding authors.

AUTHOR CONTRIBUTIONS

QB and MG did the experimental work. SA and SR supervised the work. All co-authors analyzed the results and wrote the paper.

FUNDING

This study was financially supported by ADEME (The French Environment and Energy Management Agency) and CEA (French Alternative Energy and Atomic Energy Commission). The study was also partly funded by The Carnot Institute Energies du Futur (REACSOL project 2014–2016).

REFERENCES

André, L., Abanades, S., and Cassayre, L. (2018). Mixed metal oxide systems applied to thermochemical storage of solar energy: benefits of secondary metal addition in Co and Mn oxides and contribution of thermodynamics. *Appl. Sci.* 8:2618. doi: 10.3390/app8122618

Billaud, J., Valin, S., Peyrot, M., and Salvador, S. (2016). Influence of H_2O, CO_2 and O_2 addition on biomass gasification in entrained flow reactor conditions: experiments and modelling. *Fuel* 166, 166–178. doi: 10.1016/j.fuel.2015.10.046

Boujjat, H., Rodat, S., Chuayboon, S., and Abanades, S. (2019). Experimental and numerical study of a directly irradiated hybrid solar/combustion spouted bed reactor for continuous steam gasification of biomass. *Energy* 189:116118. doi: 10.1016/j.energy.2019.116118

Charvin, P., Abanades, S., Flamant, G., and Lemort, F. (2007). Two-step water splitting thermochemical cycle based on iron oxide redox pair for solar hydrogen production. *Energy* 32, 1124–1133. doi: 10.1016/j.energy.2006.07.023

Cheynet, B., and Chevalier, P. (2002). Thermosuite. *Calphad* 26, 167–174. doi: 10.1016/S0364-5916(02)00033-0

Chuayboon, S., Abanades, D. S., and Rodat, D. S. (2019). Stepwise solar methane reforming and water-splitting via lattice oxygen transfer in iron and cerium *Oxides* 12:1900415. doi: 10.1002/ente.201900415

Chuayboon, S., Abanades, S., and Rodat, S. (2018). Solar chemical looping gasification of biomass with the ZnO/Zn redox system for syngas and zinc production in a continuously-fed solar reactor. *Fuel* 215, 66–79. doi: 10.1016/j.fuel.2017.11.021

Codina Gironès, V., Peduzzi, E., Vuille, F., and Maréchal, F. (2018). On the assessment of the CO_2 mitigation potential of woody biomass. *Front. Energy Res.* 5:37. doi: 10.3389/fenrg.2017.00037

Dupont, C., Boissonnet, G., Seiler, J.-M., Gauthier, P., and Schweich, D. (2007). Study about the kinetic processes of biomass steam gasification. *Fuel* 86, 32–40. doi: 10.1016/j.fuel.2006.06.011

Fernández-González, D., Ruiz-Bustinza, I., González-Gasca, C., Piñuela Noval, J., Mochón-Castaños, J., Sancho-Gorostiaga, J., et al. (2018). Concentrated solar energy applications in materials science and metallurgy. *Sol. Energy* 170, 520–540. doi: 10.1016/j.solener.2018.05.065

Gauthier, G., Melkior, T., Grateau, M., Thiery, S., and Salvador, S. (2013). Pyrolysis of centimetre-scale wood particles: new experimental developments and results. *J. Anal. Appl. Pyrolysis* 104, 521–530. doi: 10.1016/j.jaap.2013.05.017

Gokon, N., Izawa, T., and Kodama, T. (2015). Steam gasification of coal cokes by internally circulating fluidized-bed reactor by concentrated Xe-light radiation for solar syngas production. *Energy* 79, 264–272. doi: 10.1016/j.energy.2014.11.012

Hacker, V., Fankhauser, R., Faleschini, G., Fuchs, H., Friedrich, K., Muhr, M., et al. (2000). Hydrogen production by steam–iron process. 5, 531–535. doi: 10.1016/S0378-7753(99)00458-9

Hathaway, B. J., Kittelson, D. B., and Davidson, J. H. (2014). Development of a molten salt reactor for solar gasification of biomass. *Energy Procedia* 49, 1950–1959. doi: 10.1016/j.egypro.2014.03.207

Huang, Z., He, F., Zhao, K., Feng, Y., Zheng, A., Chang, S., et al. (2014). Natural iron ore as an oxygen carrier for biomass chemical looping gasification in a fluidized bed reactor. *J. Therm. Anal. Calorim.* 116, 1315–1324. doi: 10.1007/s10973-013-3630-1

Huang, Z., He, F., Zhu, H., Chen, D., Zhao, K., Wei, G., et al. (2015). Thermodynamic analysis and thermogravimetric investigation on chemical looping gasification of biomass char under different atmospheres with Fe_2O_3 oxygen carrier. *Appl. Energy* 157, 546–553. doi: 10.1016/j.apenergy.2015.03.033

IEAGHG (2013). *2013-04 Iron and Steel CCS Study (Techno-Economics Integrated Steel Mill).* Available online at: https://ieaghg.org/publications/technical-reports/reports-list/9-technical-reports/1001-2013-04-iron-and-steel-ccs-study-techno-economics-integrated-steel-mill (accessed January 17, 2020).

Krenzke, P. T., Fosheim, J. R., and Davidson, J. H. (2017). Solar fuels via chemical-looping reforming. *Sol. Energy* 156, 48–72. doi: 10.1016/j.solener.2017.05.095

Kumar, A., Jones, D. D., and Hanna, M. A. (2009). Thermochemical biomass gasification: a review of the current status of the technology. *Energies* 2, 556–581. doi: 10.3390/en20300556

Loutzenhiser, P. G., and Muroyama, A. P. (2017). A review of the state-of-the-art in solar-driven gasification processes with carbonaceous materials. *Sol. Energy* 156, 93–100. doi: 10.1016/j.solener.2017.05.008

Nzihou, A., Flamant, G., and Stanmore, B. (2012). Synthetic fuels from biomass using concentrated solar energy - a review. *Energy* 42, 121–131. doi: 10.1016/j.energy.2012.03.077

Piatkowski, N., Wieckert, C., Weimer, A. W., and Steinfeld, A. (2011). Solar-driven gasification of carbonaceous feedstock—a review. *Energy Env. Sci* 4, 73–82. doi: 10.1039/C0EE00312C

Sarafraz, M. M., Jafarian, M., Arjomandi, M., and Nathan, G. J. (2017a). Potential use of liquid metal oxides for chemical looping gasification: a thermodynamic assessment. *Appl. Energy* 195, 702–712. doi: 10.1016/j.apenergy.2017.03.106

Sarafraz, M. M., Jafarian, M., Arjomandi, M., and Nathan, G. J. (2017b). The relative performance of alternative oxygen carriers for liquid chemical looping combustion and gasification. *Int. J. Hydrog. Energy* 42, 16396–16407. doi: 10.1016/j.ijhydene.2017.05.116

Wu, Z., Zhang, B., Wu, S., Li, G., Zhao, S., Li, Y., et al. (2019). Chemical looping gasification of lignocellulosic biomass with iron-based oxygen carrier: Products distribution and kinetic analysis on gaseous products from cellulose. *Fuel Process. Technol.* 193, 361–371. doi: 10.1016/j.fuproc.2019.05.021

Yang, J. B., Cai, N. S., and Li, Z. S. (2008). Hydrogen production from the steam-iron process with direct reduction of iron oxide by chemical looping combustion of coal char. *Energy Fuels* 22, 2570–2579. doi: 10.1021/ef800014r

Yu, Z., Yang, Y., Yang, S., Zhang, Q., Zhao, J., Fang, Y., et al. (2019). Iron-based oxygen carriers in chemical looping conversions: a review. *Carbon Resour. Convers.* 2, 23–34. doi: 10.1016/j.crcon.2018.11.004

Zeng, J., Xiao, R., Zhang, S., Zhang, H., Zeng, D., Qiu, Y., et al. (2018). Identifying iron-based oxygen carrier reduction during biomass chemical looping gasification on a thermogravimetric fixed-bed reactor. *Appl. Energy* 229, 404–412. doi: 10.1016/j.apenergy.2018.08.025

Zgraggen, A., and Steinfeld, A. (2008). Hydrogen production by steam-gasification of carbonaceous materials using concentrated solar energy – V. Reactor modeling, optimization, and scale-up. *Int. J. Hydrog. Energy* 33, 5484–5492. doi: 10.1016/j.ijhydene.2008.07.047

Zhao, X., Zhou, H., Sikarwar, V. S., Zhao, M., Park, A.-H. A., Fennell, P. S., et al. (2017). Biomass-based chemical looping technologies: the good, the bad and the future. *Energy Environ. Sci.* 10, 1885–1910. doi: 10.1039/C6EE03718F

Zhu, M., Song, Y., Chen, S., Li, M., Zhang, L., and Xiang, W. (2019). Chemical looping dry reforming of methane with hydrogen generation on Fe2O3/Al2O3 oxygen carrier. *Chem. Eng. J.* 368, 812–823. doi: 10.1016/j.cej.2019.02.197

Conflict of Interest: The authors declare that the research was conducted in the absence of any commercial or financial relationships that could be construed as a potential conflict of interest.